NANOSYSTEMS:
PHYSICS, CHEMISTRY, MATHEMATICS

Perminova D.A., et al. *Nanosystems: Phys. Chem. Math.*, 2025, **16** (4), 467–471.
http://nanojournal.ifmo.ru
DOI 10.17586/2220-8054-2025-16-4-467-471

Original article

Surface electronic structure of $TbIr_2Si_2$ antiferromagnet

D. A. Perminova[1,a], I. A. Shvets[2,b], D. Yu. Usachov[2,c],
D. V. Vyalykh[2,d], S. V. Eremeev[1,2,e]

[1]Institute of Strength Physics and Materials Science, Russian Academy of Sciences, 634055 Tomsk, Russia
[2]St. Petersburg State University, 199034 St. Petersburg, Russia

[a]homyak.22.07.1999@mail.ru, [b]shvets_ia@mail.ru, [c]dmitry.usachov@spbu.ru,
[d]denis.vyalikh@gmail.com, [e]eremeev@ispms.ru

Corresponding author: D. A. Perminova, homyak.22.07.1999@mail.ru

ABSTRACT By means of *ab initio* density functional theory (DFT) calculations, we examined the surface electronic structure of the $TbIr_2Si_2$ antiferromagnet, which is distinguished by the out-of-plane alignment of Tb $4f$ moments and a high Néel temperature. We analyzed the interplay between the spin-orbit and exchange interactions and their effect on the dispersion of surface states resided in the projected band gap around the $\bar{\mathrm{M}}$ point of the surface Brillouin zone, and compared our theoretical findings with low-temperature angle-resolved photoemission spectroscopy (ARPES) measurements.

KEYWORDS magnetic rare-earth intermetallic materials, surface electronic structure, density functional theory, angle-resolved photoemission spectroscopy.

ACKNOWLEDGEMENTS The authors acknowledge support from the Saint-Petersburg State University (project 125022702939-2). D.A.P. and S.V.E. acknowledge support from the Government research assignment for ISPMS SB RAS (project FWRW-2022-0001).

FOR CITATION Perminova D.A., Shvets I.A., Usachov D.Yu., Vyalykh D.V., Eremeev S.V. Surface electronic structure of $TbIr_2Si_2$ antiferromagnet. *Nanosystems: Phys. Chem. Math.*, 2025, **16** (4), 467–471.

1. Introduction

For a long time, rare-earth (RE) intermetallic materials have attracted considerable interest because of their exotic properties at low temperatures, which include complex magnetic phases, heavy-fermion states, the Kondo behaviour and others [1, 2]. Of particular interest are the intermetallics with REX_2Si_2 stoichiometry [3–10], where the strength of the Rashba spin-orbit coupling in the surface states can be tuned by choosing suitable transition metal atoms. It increases by exchanging X element from $3d$ row, where the Rashba effect is relatively weak, to $4d$ and $5d$, where it should be the largest [8]. While materials with RE=Eu, Gd and their surface electronic structure have been well explored by means of angle- and spin-resolved photoemission spectroscopy (ARPES and SARPES) and complementary theoretical calculations, the terbium-based counterparts remain insufficiently studied.

This work is devoted to study of $TbIr_2Si_2$, currently underexplored antiferromagnet with a fairly high Néel temperature (80 K) [11]. In contrast to related $GdIr_2Si_2$ compound [8], in which RE atom magnetic moments are oriented in-plane, the $TbIr_2Si_2$ is characterized by the out-of-plane magnetic moments alignment. The cleavage plane in REX_2Si_2 lies along the RE-Si bond, thus ensuring the formation of rare-earth- and silicon-terminated (001) surfaces. In this work, we study the surface electronic structure of the silicon termination by means of the density functional theory (DFT) calculations, analyzing the effects of spin-orbit and exchange interactions on the dispersion of surface states. Finally, we compare the calculation results with low-temperature ARPES measurements.

2. Methods

Electronic structure calculations were carried out within the DFT using the projector augmented-wave (PAW) method [12, 13] as implemented in the VASP package [13, 14]. The exchange-correlation energy was treated using the generalized gradient approximation (GGA) [15] for most calculations. The standard Tb potential in which the $4f$ electrons are treated as valence states was used for spin-polarized calculations of magnetic phases. For paramagnetic phase calculations we used Tb potential in which $4f$ electrons are treated as core states. To correctly describe the highly correlated Tb-$4f$ electrons, we included the correlation effects within both the HSE06 screened hybrid functional [16] and the GGA+U method [17]. The values of U and J were taken to be of 6.7 eV and 0.7 eV, respectively, which give a good agreement with HSE06 band structure. Additionally, we used the Slater-type DFT-1/2 self-energy correction method [18, 19] with a partially (quaternary) ionized silicon potential for better describing the hybridization between deep Tb-f and Si-p_{xy} orbitals. The experimental lattice constants ($a = 4.143$, $c = 10.155$ Å) were adopted from Ref. [20]. The atomic positions were optimized by minimizing forces acting on the atoms.

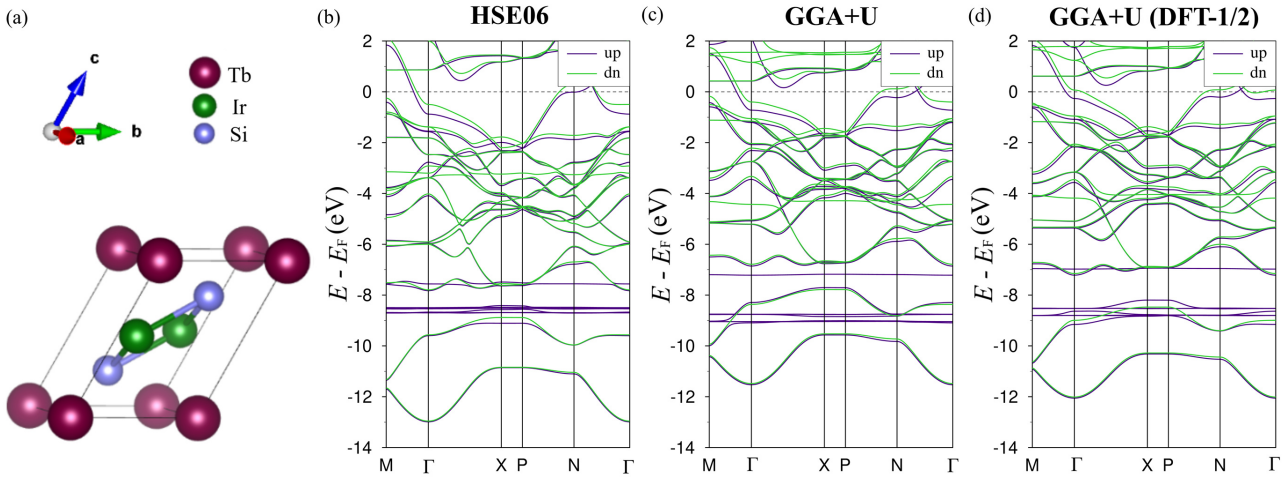

FIG. 1. (a) Primitive unit cell of $TbIr_2Si_2$. Bulk band spectrum of $TbIr_2Si_2$ in ferromagnetic phase calculated (b) with HSE06 screened hybrid functional, (c) within GGA+U approach, and (d) within GGA+U with additional partial ionization of the Si potential within the Slater-type DFT-1/2 self-energy correction method. Purple and green lines highlight the spin-up and spin-down states, respectively

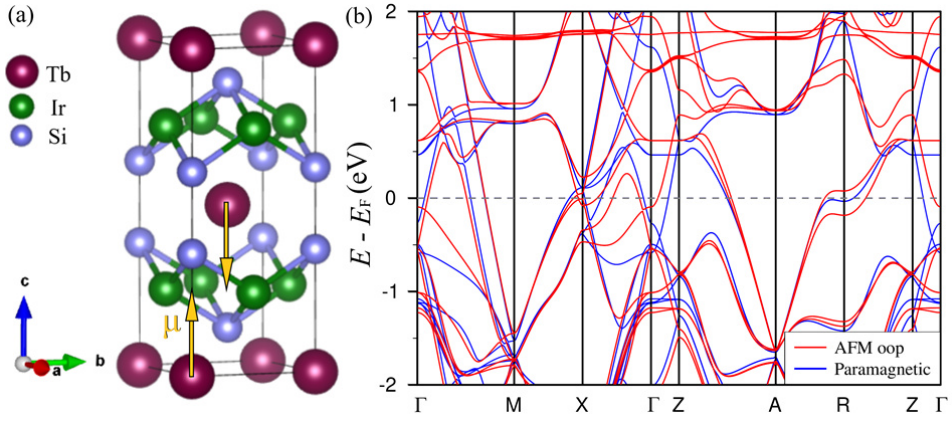

FIG. 2. (a) Tetragonal unit cell of $TbIr_2Si_2$ in antiferromagnetic phase. Yellow arrows indicate the directions of magnetic moments on Tb atoms. (b) Bulk band spectrum of $TbIr_2Si_2$: antiferromagnetic phase with out-of-plane (oop) magnetic ordering (red lines) and paramagnetic phase (blue lines)

The surface electronic structure was studied within the framework of the slab model. The slab was constructed in such a way that its top and bottom surfaces had a silicon termination and the slab thickness amounts of 39 atomic layers. Surface electronic structure calculations were performed for both paramagnetic and magnetic states, with and without taking into account the spin-orbit coupling.

All presented ball-and-stick atomic structures were visualized with VESTA [21].

A detailed method for obtaining high-quality $TbIr_2Si_2$ single crystals is described in Ref. [20]. ARPES experiments were carried out at the BESSY II synchrotron at the "One-Cubed ARPES" station.

3. Results

The screened hybrid functional HSE06, which gives an accurate description of the electronic structure, is, however, resource-consuming. For this reason, we use it only to select the optimal Hubbard U and Hund J parameters in the GGA+U method. To this end, we carried out a series of calculations within the primitive cell (Fig. 1 (a)) for the artificial FM phase and found that U and J equaled to 6.7 and 0.7 eV, respectively, satisfactorily describe the position of the terbium f-band (Fig. 1 (b,c)). However, in contrast to the HSE06 spectrum in which dispersionless f band at ≈ -8.5 eV almost does not hybridize with the deeper states, in GGA+U it intersects these dispersed states. These deep states are of Si p_{xy} character and to improve their description we applied the DFT-1/2 method (Fig. 1 (d)). All further calculations were carried out in this approach with the established parameters.

The ground magnetic state of the $TbIr_2Si_2$ is an interlayer antiferromagnetic phase characterized by an easy axis pointed perpendicular to the magnetic layers [11]. The magnetic tetragonal unit cell containing two formula units is shown in Fig. 2 (a). The calculated bulk electronic structure of the AFM $TbIr_2Si_2$ is demonstrated in Fig. 2 (b) in comparison

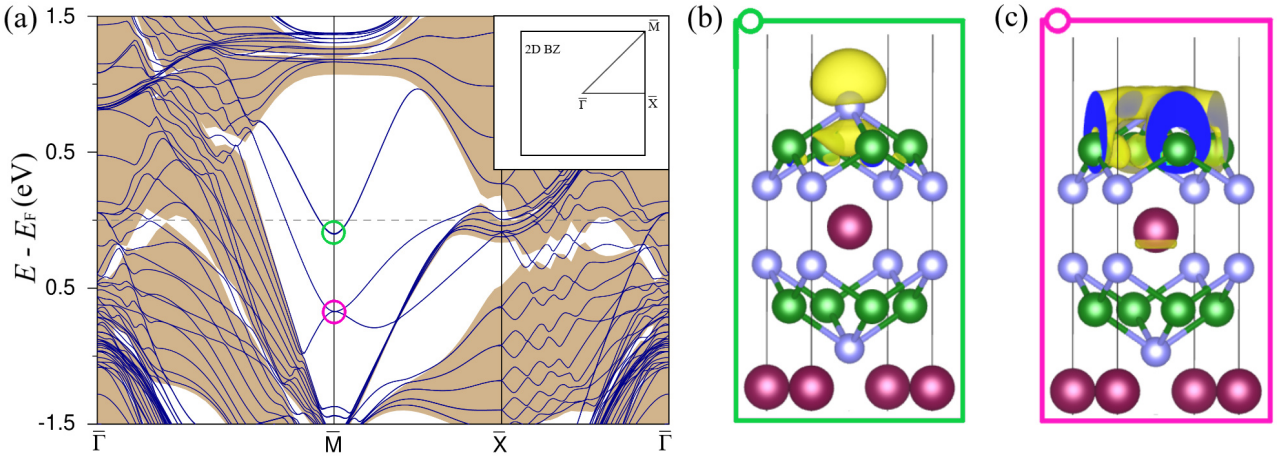

FIG. 3. (a) Electronic structure of the silicon-terminated surface of $TbIr_2Si_2$ in paramagnetic phase calculated without taking the spin-orbit coupling into account. The shaded region corresponds to the projection of the bulk band structure. Inset shows the 2D surface Brillouin zone and high-symmetry directions along which the band structure is calculated. (b, c) Spatial distribution of the surface states, marked with circles of corresponding color (green or pink) in panel (a)

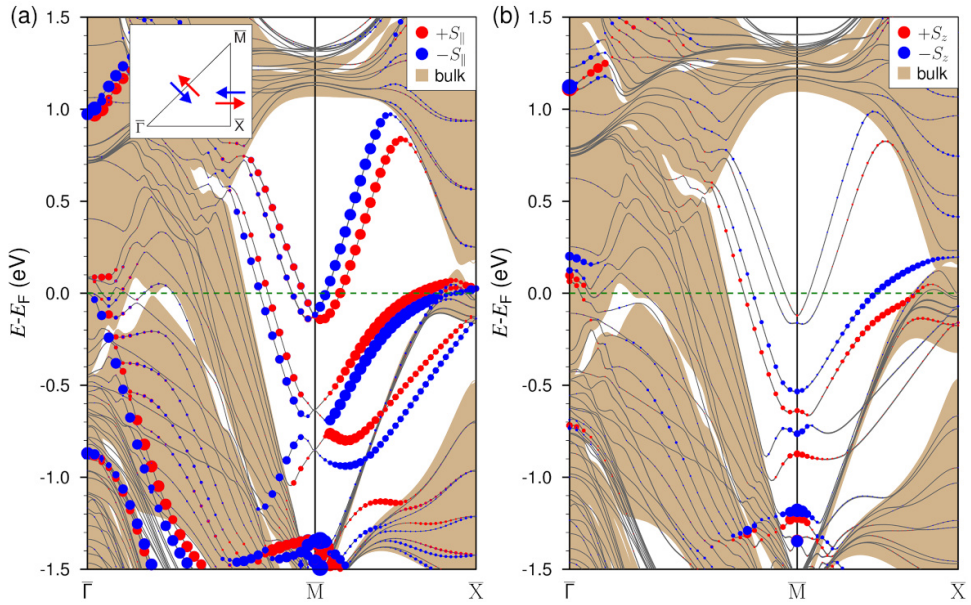

FIG. 4. (a) Relativistic electronic structure of the silicon-terminated surface of $TbIr_2Si_2$ in the paramagnetic phase calculated along the $\bar{\Gamma}-\bar{\mathrm{M}}-\bar{\mathrm{X}}$ path of the surface Brillouin zone. Shaded area corresponds to the projection of the bulk band structure. Red and blue circles show the in-plain spin components ($\pm S_{\parallel}$) for the states localized in the four topmost layers. Green dashed line marks position of the Fermi level. Inset schematically shows alignment of $S_{\parallel}$ in the $\bar{\mathrm{M}}-\bar{\Gamma}$ and $\bar{\mathrm{M}}-\bar{\mathrm{X}}$ directions. (b) Surface electronic structure of $TbIr_2Si_2$ in AFM phase. Red and blue circles show positive and negative, respectively, out-of-plane (S_z) spin components of the surface states

with the spectrum of the paramagnetic phase. This comparison clearly shows the influence of the $f-d$ hybridization of the terbium orbitals on the electronic spectrum near the Fermi level. As can be seen, differences in the spectra near the Fermi level, mainly at the X and R points, that indicate that the f-electrons of terbium affect its d-orbitals, which hybridize with the d-orbitals of iridium, magnetizing them.

We begin our consideration of the surface electron spectrum from the paramagnetic phase, neglecting the spin-orbit interaction (Fig. 3). As can be seen in Fig. 3 (a), the metallic bulk spectrum of $TbIr_2Si_2$ contains a vast gap centered at the $\bar{\mathrm{M}}$ point of the surface Brillouin zone (see inset in Fig. 3 (a)), which provides a room for a series of surface states. The upper surface state, lying near the Fermi level, is almost entirely localized on the outer silicon atom and mostly formed by its p_z orbitals (Fig. 3 (b)). The two lower states, with electron and hole dispersions, are degenerate at the $\bar{\mathrm{M}}$ point at an energy of ≈ -0.7 eV and both are mainly formed by d orbitals of the iridium atoms (Fig. 3 (c)).

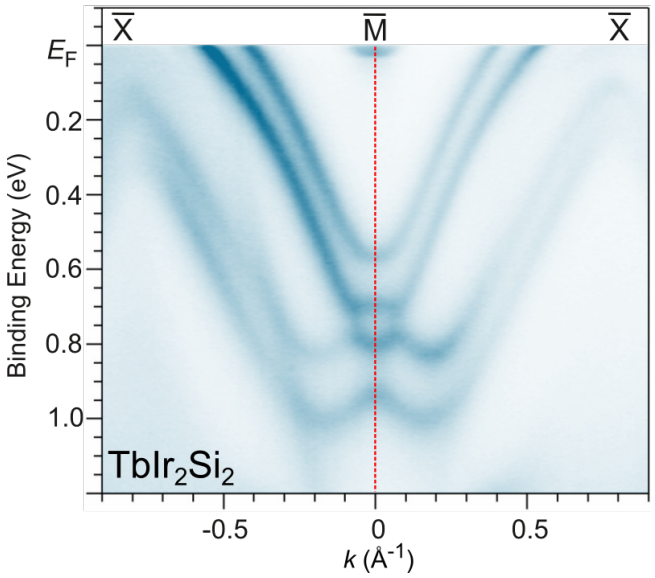

FIG. 5. ARPES spectrum of the Si-terminated surface of $TbIr_2Si_2$ measured at temperature of 7 K in the vicinity of the $\bar{\mathrm{M}}$ point.

Remaining in the paramagnetic phase, switching-on the spin-orbit interaction results in the emergence of the Rashba-type spin splitting, as well as lifting the degeneracy of the two lower energy bands (Fig. 4 (a)). In this instance, the splitting of the spin subbands is particularly noteworthy, especially concerning the lower energy states, which are closely related to the substantial atomic spin-orbit coupling on $5d$ iridium. In the low-temperature limit, when the AFM magnetic order in $TbIr_2Si_2$ is established, in addition to the spin-orbit interaction, the exchange interaction arises, which leads to the lifting the Kramers degeneracy of the Rashba states at the $\bar{\mathrm{M}}$ point and appearance of S_z spin component on the surface states (Fig. 4 (b)). At the same time, the exchange splitting in the surface state lying at the Fermi level is about 50 meV, while in the deep-lying states it reaches 150 meV. Such a significant difference is due to the different localization of these states. As was pointed above, the surface state lying at the Fermi level is formed mainly by the orbitals of the surface silicon atom and its wave function weakly penetrates deep under the surface, so its hybridization with magnetic atoms is small. In the low-lying states, formed primarily by the d orbitals of iridium, their strong hybridization with orbitals of magnetic Tb occurs.

The spectrum in the vicinity of the $\bar{\mathrm{M}}$ point obtained using the angle-resolved photoemission spectroscopy measurements at 7 K is shown in Fig. 5. Comparing the calculated surface band structure of the $TbIr_2Si_2$ antiferromagnet with low-temperature measurements, one can see that the theoretical spectrum demonstrates good agreement with the ARPES data. The calculations reproduce the dispersion of the surface states and their spin splittings. Small differences in the positions of the surface states are most likely due to structural factors associated with atomic relaxation in the calculation. Alongside, the theoretical calculations make it possible to trace the effects of spin-orbit and exchange interactions separately and explain the large difference in the exchange splitting of different surface states on the base of an analysis of their spatial localization and, consequently, the different hybridization of these states with the orbitals of the magnetic atom.

4. Conclusion

In summary, utilizing the density functional theory calculations, we have studied bulk and surface electronic structure of the $TbIr_2Si_2$ antiferromagnet. The bulk electronic structure calculations using screened hybrid functional allowed us to establish accurate description of the bands and develop appropriate Hubbard parameters for simplified GGA+U model. Consideration of paramagnetic and antiferromagnetic phases allowed us to distinguish the effects of spin-orbit and magnetic exchange interactions on the electronic structure of the material. The theoretical surface spectrum of the $TbIr_2Si_2$ antiferromagnet was found to be in an excellent agreement with high-accuracy low-temperature ARPES measurements. Analysis of the spatial localization of the surfaces states and their hybridization with orbitals of magnetic atoms allows us to explain the observed features of the spectrum.

References

[1] Stewart G.R. Heavy-fermion systems. *Rev. Mod. Phys.*, Oct 1984, **56**, P. 755–787.
[2] Si Q., Steglich F. Heavy Fermions and Quantum Phase Transitions. *Science*, Sep 2010, **329**, P. 1161–1166.
[3] Chikina A., Höppner M., Seiro S., Kummer K., Danzenbächer S., Patil S., Generalov A., Güttler M., Kucherenko Y., Chulkov E.V., et al. Strong ferromagnetism at the surface of an antiferromagnet caused by buried magnetic moments. *Nature communications*, 2014, **5**(1), P. 3171.

[4] Güttler M., Generalov A., Otrokov M.M., Kummer K., Kliemt K., Fedorov A., Chikina A., Danzenbächer S., Schulz S., Chulkov E.V., Koroteev Y.M., Caroca-Canales N., Shi M., Radovic M., Geibel C., Laubschat C., Dudin P., Kim T.K., Hoesch M., Krellner C., Vyalikh D.V. Robust and tunable itinerant ferromagnetism at the silicon surface of the antiferromagnet $GdRh_2Si_2$. *Scientific Reports*, Apr. 2016, **6**, P. 24254.

[5] Generalov A., Otrokov M.M., Chikina A., Kliemt K., Kummer K., Höppner M., Güttler M., Seiro S., Fedorov A., Schulz S., Danzenbächer S., Chulkov E.V., Geibel C., Laubschat C., Dudin P., Hoesch M., Kim T., Radovic M., Shi M., Plumb N.C., Krellner C., Vyalikh D.V. Spin Orientation of Two-Dimensional Electrons Driven by Temperature-Tunable Competition of Spin-Orbit and Exchange-Magnetic Interactions. *Nano Letters*, 2017, **17**(2), P. 811–820.

[6] Vyazovskaya A.Y., Otrokov M.M., Koroteev Y.M., Kummer K., Güttler M., Vyalikh D.V., Chulkov E.V. Origin of two-dimensional electronic states at Si- and Gd-terminated surfaces of $GdRh_2Si_2$(001). *Phys. Rev. B*, Aug 2019, **100**, P. 075140.

[7] Schulz S., Nechaev I., Guttler M., Poelchen G., Generalov A., Danzenbacher S., Chikina A., Seiro S., Kliemt K., Vyazovskaya A., Kim T., Dudin P., Chulkov E., Laubschat C., Krasovskii E., Geibel C., Krellner C., Kummer K., Vyalikh D. Emerging $2d$-ferromagnetism and strong spin-orbit coupling at the surface of valence-fluctuating $EuIr_2Si_2$. *npj Quantum Materials*, 06 2019, **4**, P. 26.

[8] Schulz S., Vyazovskaya A.Y., Poelchen G., Generalov A., Güttler M., Mende M., Danzenbächer S., Otrokov M.M., Balasubramanian T., Polley C., Chulkov E.V., Laubschat C., Peters M., Kliemt K., Krellner C., Usachov D.Y., Vyalikh D.V. Classical and cubic Rashba effect in the presence of in-plane $4f$ magnetism at the iridium silicide surface of the antiferromagnet $GdIr_2Si_2$. *Phys. Rev. B*, Jan 2021, **103**, P. 035123.

[9] Generalov A., Falke J., Nechaev I.A., Otrokov M.M., Güttler M., Chikina A., Kliemt K., Seiro S., Kummer K., Danzenbächer S., Usachov D., Kim T.K., Dudin P., Chulkov E.V., Laubschat C., Geibel C., Krellner C., Vyalikh D.V. Strong spin-orbit coupling in the noncentrosymmetric Kondo lattice. *Phys. Rev. B*, Sep 2018, **98**, P. 115157.

[10] Vyazovskaya A.Y., Kuznetsov V.M. Spin-orbit interaction effect on surface electronic structure of GdX_2Si_2 compound. *Russian Physics Journal*, 2021, **64**, P. 1451–1459.

[11] Shigeoka T., Kurata Y., Nakata T., Fujiwara T., Matsubayashi K., Uwatoko Y. Crystal field effects in polymorphic compound $TbIr_2Si_2$. *Physics Procedia*, 2015, **75**, P. 837–844. 20th International Conference on Magnetism, ICM 2015.

[12] Blöchl P.E. Projector augmented-wave method. *Phys. Rev. B*, Dec 1994, **50**, P. 17953–17979.

[13] Kresse G., Joubert D. From ultrasoft pseudopotentials to the projector augmented-wave method. *Phys. Rev. B*, Jan 1999, **59**, P. 1758–1775.

[14] Kresse G., Furthmüller J. Efficient iterative schemes for ab initio total-energy calculations using a plane-wave basis set. *Phys. Rev. B*, Oct 1996, **54**, P. 11169–11186.

[15] Perdew J.P., Burke K., Ernzerhof M. Generalized gradient approximation made simple. *Phys. Rev. Lett.*, Oct 1996, **77**, P. 3865–3868.

[16] Krukau A.V., Vydrov O.A., Izmaylov A.F., Scuseria G.E. Influence of the exchange screening parameter on the performance of screened hybrid functionals. *The Journal of chemical physics*, 2006, **125**(22), P. 224106.

[17] Anisimov V.I., Zaanen J., Andersen O.K. Band theory and Mott insulators: Hubbard U instead of Stoner I. *Phys. Rev. B*, Jul 1991, **44**, P. 943–954.

[18] Ferreira L.G., Marques M., Teles L.K. Approximation to density functional theory for the calculation of band gaps of semiconductors. *Phys. Rev. B*, Sep 2008, **78**, P. 125116.

[19] Ferreira L.G., Marques M., and Teles L.K. Slater half-occupation technique revisited: the LDA-1/2 and GGA-1/2 approaches for atomic ionization energies and band gaps in semiconductors. *AIP Advances*, Sep 2011, **1**, P. 032119.

[20] Kliemt K., Peters M., Feldmann F., Kraiker A., Tran D.-M., Rongstock S., Hellwig J., Witt S., Bolte M., Krellner C. Crystal growth of materials with the $ThCr_2Si_2$ structure type. *Cryst. Res. Technol.*, 2020, **55**(2), P. 1900116.

[21] Momma K., Izumi F. *VESTA3* for three-dimensional visualization of crystal, volumetric and morphology data. *Journal of Applied Crystallography*, Dec 2011, **44**, P. 1272–1276.

Submitted 2 July 2025; revised 20 July 2025; accepted 21 July 2025

Information about the authors:

D. A. Perminova – Institute of Strength Physics and Materials Science, Russian Academy of Sciences, 634055 Tomsk, Russia; homyak.22.07.1999@mail.ru

I. A. Shvets – St. Petersburg State University, 199034 St. Petersburg, Russia; ORCID 0000-0003-1385-2176; shvets_ia@mail.ru

D. Yu. Usachov – St. Petersburg State University, 199034 St. Petersburg, Russia; ORCID 0000-0003-0390-0007; dmitry.usachov@spbu.ru

D. V. Vyalykh – St. Petersburg State University, 199034 St. Petersburg, Russia; denis.vyalikh@gmail.com

S. V. Eremeev – Institute of Strength Physics and Materials Science, Russian Academy of Sciences, 634055 Tomsk, Russia; St. Petersburg State University, 199034 St. Petersburg, Russia; ORCID 0000-0002-9477-3017; eremeev@ispms.ru

Conflict of interest: the authors declare no conflict of interest.